Biophysics

http://www.aimspress.com/journal/biophysics

AIMS Biophysics, 12(4): 499−509.
DOI: 10.3934/biophy.2025024
Received: 01 September 2025
Revised: 03 October 2025
Accepted: 10 October 2025
Published: 14 October 2025

Review

CMOS cameras: state-of-the-art technology for neuronal functional imaging with high spatiotemporal resolution

Marco Canepari[1,2,*]

[1] Univ. Grenoble Alpes, CNRS, LIPhy UMR5588, F-38000 Grenoble, France
[2] Institut National de la Santé et Recherche Médicale, Paris, France

* **Correspondence:** Email: marco.canepari@univ-grenoble-alpes.fr.

Abstract: In the last decade, complementary metal-oxide semi-conductor (CMOS) cameras became the state-of-the-art technology in many biological applications, and the ability to reach high acquisition rates represents one of the characteristics that outperform previous technologies. In this review, I concentrated on neuronal functional imaging (voltage and/or ions) that requires recording fluorescence from multiples sites of a neuron or of a network at kHz rates to sample signals associated with neuronal excitability. After introducing the physical constrains of this type of imaging and reviewing the technologies used in the past, I analysed how CMOS can address the challenge of neuronal functional imaging. I focused on the characteristics of two CMOS cameras that are in use in my laboratory: DaVinci2K and Kinetix. DaVinci2K achieves high acquisitions rates at 14-bit depth by using parallel processing from 16 sub-sensors whereas Kinetix achieves higher spatiotemporal resolution by sampling fluorescence at 8-bit depth, but at the cost of decreasing the dynamic range which represents a limitation in several experimental scenarios. I present comparable membrane potential imaging recordings of action potentials from the axon initial segment, which were achieved at 20 kHz with the two cameras. Finally, I conclude the review with some perspective considerations on future availability of CMOS cameras that may overcome the performance of present devices and the limitations in developing optimal devices for biological and biomedical applications.

Keywords: CMOS; imaging; neuron; fluorescence; membrane potential

1. Introduction

When imaging ion or membrane potential (V_m) transients, representing most signals reporting physiological activity in living neurons [1], the ability to detect and potentially quantify a signal depends on three mutually correlated physical constrains. First, if the signal originates from a small site, the optical resolution must permit the clear discrimination of photons from that site. In wide-field fluorescence microscopy, this is limited by the Abbé resolution [2] given by the equation:

$$\rho = 1.22 \cdot \lambda / (2 \cdot \mathrm{NA}) \quad (1)$$

where λ is the emitted wavelength and NA is the numerical aperture of the used objective. ρ is an ideal value which is less than 1 μm for all visible wavelengths, but it is worsened by light scattering in tissues between the fluorescence source and the objective. It can be improved using confocal [3] or two-photon (2P, [4,5]) imaging. The second constrain is related to the temporal resolution. If a signal is fast and must be resolved in all its components, the acquisition rate of fluorescence sampling must be at least double than the highest relevant frequency component of the signal, according to the Nyquist theorem. The last constrain is given by the size of the signal, which must be discriminated above the intrinsic photon noise of the fluorescence. Precisely, if the transient corresponds to the fractional change of fluorescence $\Delta F/F_0$, the signal-to-noise ratio (SNR) of a transient (ΔN_{ph}) measured from an initial number of photons (N_{ph}) is given by the equation:

$$\mathrm{SNR} = \Delta N_{ph} / \sqrt{N_{ph}}. \quad (2)$$

It follows that the measurement of a given $\Delta F/F_0$ signal must be done from a minimal N_{ph} value that increases with the size of the fluorescence source and with the time window at which fluorescence is collected, which limits the acquisition rate of fluorescence sampling. Beyond these physical constraints, further limitations are set by the device used to record fluorescence.

The need of recording fluorescence transients from multiple sites with 0.1−10 kHz temporal resolution emerged in the last two decades of the twentieth century. Initially, photodiode arrays were utilized as optimal detectors for recording voltage-sensitive dye (VSD) membrane potential (V_m) signals (see for example [6–9]). Starting from the nineties of the past century, charge coupled devices (CCDs) became the most used technology (see for example [10−14]). With CCD cameras, it is possible to increase acquisition rates by reducing the number of sampled pixels in one dimension and by performing online binning (see for example [15−17]). Thus, to reconstruct V_m and ion transients associated with neuronal action potentials (APs) or synaptic potentials, fluorescence was measured at 2 kHz from 6400 pixels (see for example [18−20]) or at 5−20 kHz from ~ 100−1500 pixels (see for example [21−26]) using a CCD camera where photoelectrons were sampled in parallel by four processors at 14-bit depth. In terms of speed with respect to number of pixels, i.e., "spatiotemporal resolution", complementary metal-oxide semi-conductor (CMOS) devices appeared to be superior and commercial scientific CMOS (sCMOS) cameras started being the preferred option in the new century (see for example [27−36]). Moreover, in CCD cameras, the charge in each pixel is shifted and amplified, and in CMOS cameras, each pixel has its own amplifier resulting in faster read-out. Notably, given the larger spatial resolution, CMOS cameras are also more suitable for multiple microscopy approaches; they can be utilized to collect fluorescence excited by wide-filed illumination [36]; they can be used for volumetric imaging by as light sheet microscopy [27]; or they can be exploited for fast confocal microscopy by inserting a spinning disk in the illumination/emission pathway [28]. More than a decade since their introduction was necessary to affirm CMOS cameras as state-of-art technology, replacing CCDs in applications where combination of high sensitivity and spatiotemporal resolutions are required. In this review, I aim to report the requirements for neuronal functional imaging with respect to what is offered by state-of-the-art CMOS cameras. I use measurements, obtained with two cameras, to show the present capabilities of CMOS devices.

2. Technical aspects and two examples of commercially available CMOS cameras

From the considerations taken above, I use as refence values 1 μm for the size covered by a pixel and 1 for the NA of the objective used to visualise the neuronal tissue (see Equation 1). Water immersion objectives with NA = ~ 1, normally used for patch clamp recordings, exist from several companies at 40X, 60X and 100X magnification. To obtain 1 μm/pixel using these lenses, cameras must have pixels of 40 μm, 60 μm, and 100 μm respectively. However, de-magnifying lenses (typically 0.25−0.5X) can be used to adapt to the sensor. Expensive objectives with lower magnification and NA = ~ 1 exist. For instance, a Nikon 25X objective with NA = 1.1 has been used to image and patch in the mossy fibre pathway in hippocampal slices [37,38]. Using this objective and a 0.25X de-magnifying lens, 1 μm/pixel would be achieved with a pixel size of 4 μm only. Compared to CCD cameras, CMOS cameras are faster because amplification and A/D conversion, performed on the sensor, are executed independently in each pixel column. Thus, while both CCD and CMOS devices increase the acquisition rate by decreasing the vertical dimensions, CMOS cameras avoid the time necessary for the horizontal register shift of CCD cameras. Additionally, several sCMOS cameras can further increase the acquisition speed by supporting a “rolling shutter” mode, where different lines of the array are exposed at different times. This acquisition mode means that signals must be temporally oversampled in order to correlate in time different sites. Table 1 reports specifications of five commercially available CMOS cameras that were used for neuronal imaging. Two of these cameras are used in our laboratory and the other three cameras were chosen because they were from different manufacturers and because they appear to be widely utilized among those that can be considered state-of-art. Notably, the two cameras that we use have quite different specifications, which will be discussed later in this review.

Table 1. Some specifications of available CMOS cameras used in neuronal imaging.

Camera	Max QE	pixel size	full frame size	bit depth	full frame max rate	fast read noise
Edge4.2 (PCO)	70%	6.5 μm	2048 X 2048	16 (11 + 11)	100 frames/s	1.6 e^-
ORCA Flash4 (Hamamatsu)	84%	6.5 μm	2048 X 2048	8/12/16	100 frames/s	1.9 e^-
Sona (Andor)	95%	6.5 μm	2048 X 2048	11/12/16	135 frames/s	1.8 e^-
DaVinci2K (Scimeasure)	65%	15 μm	2048 X 2048	14	100 frames/s	2.8 e^-
Kinetix (Teledyne)	95%	6.5 μm	3200 X 3200	8/12/16	498 frames/s	2.0 e^-

The two first cameras on the table are front-illuminated devices, recently tested for pixel crosstalk [39], including the PCO.edge4.2 (Excelitas, Pittsburgh, PA) and the Hamamatsu Orca 4 (Hamamatsu, Japan). They have relatively high QE, pixel size of 6.5 µm, sensor of 2048 X 2048 pixels, and the ability to capture full frames at 100 Hz. PCO.edge42 samples pixels at 16-bit depth using two 11-bit A/D converters to convert signals at high and low gain and then merging the two values into a single 16-bit value. In terms of neuronal functional imaging at high spatiotemporal resolution, as an example, Orca 4 was utilised for whole-brain calcium imaging in the larval zebrafish [27] and in *Caenorhabditis elegans* [40]. The third camera in Table 1 is the back-illuminated Sona (Andor, Belfast, UK) with higher QE. This device, with sensor of 2048 X 2046 pixels of 6.5 µm size, can capture full frames at 135 Hz with 11-bit depth. A camera with a larger pixel (Sona-11, 11 µm size) is manufactured and commercialised by the same company, but this device appears to be slower (48 full frames/s with 12-bit depth). Sona-11 was utilised to image calcium *in vivo* in the primate auditory cortex [41]. Now, I analyse in detail the last two CMOS cameras in Table 1, which are used in my laboratory. DaVinci2K, manufactured and commercialised by SciMeasure (Decatur, GA), has a sensor of 2048 X 2048 relatively large pixels (15 µm), and does not use on-chip microlenses. In this device, a low read out noise is achieved by sampling at 14-bit depth, and high speed is achieved by parallel processing. The full frame is decomposed in 16 rectangles of 256 X 1048 pixels, and images in the kHz range can be acquired by sampling 2048XN rectangles in the middle of the full frame. Additionally, this camera enables on-chip binning, i.e., two complete half-columns can be binned into a single read, increasing the frame rate and the well capacity. The other camera that we use is Kinetix, commercialised by Teledyne (Waterloo, Canada). This camera has a sensor of 3200 X 3200 smaller pixels (6.5 µm) and it is back-illuminated, reaching a quantum efficiency of ~ 95%. Kinetix achieves a speed of ~ 500 Hz at full frame resolution by sampling at 8-bit depth. This digital resolution is not sufficient to resolve neuronal signals. However, at 8-bit depth, each pixel operates as quasi "photon counter" because the A/D converter saturates at ~ 200 photoelectrons. This means that 255 corresponds to 200 photoelectrons and, therefore, 1 digit = ~ 1 photoelectron. With an effective well capacity (EWC) of ~ 200 photoelectrons, performing offline binning with a factor of 2, for instance, reduces the size to 1600 X 1600 pixels but increases the depth to 10-bit and the EWC to > 800 photoelectrons. In the following section, I illustrate two representative VSD recordings obtained with the latter two CMOS devices at a very high spatiotemporal resolution.

3. Examples of recordings achieved with the two CMOS cameras

To describe the performance of the two CMOS devices in detail, we make use of comparable recordings. In our laboratory, DaVinci2K was installed in a workstation, including a spinning disk [28], but it was used without the disk in the optical path to record fluorescence transients at 10 kframes/s [31,33]. In this system, a 60X objective was used, and a 0.5X de-magnifying lens was positioned before the sensor, obtaining the image of the specimen focusing on a micrometer illustrated in Figure 1A. Since DaVinci2K has a physical pixel size of 15 µm, the effective pixel length under this configuration is ~ 0.5 µm. Kinetix was mounted in another workstation, and its ability to resolve ultrafast signals has been characterized [36]. In this system, a 60X objective was also used, but a 0.25X de-magnifying lens was positioned before the sensor, obtaining the image of the specimen focusing on a micrometer illustrated in Figure 1B. Since Kinetix has a physical pixel size of 6.5 µm, the effective pixel length under this configuration is ~ 0.43 µm. The two optical configurations were therefore comparable, except for the irrelevant reduced full field in the DaVinci2K system. Their performances could be compared by recording V_m fluorescence from the VSD JPW1114, at 20 kHz, in the axon initial segment (AIS) of neocortical layer-5 pyramidal neurons in brain slices. To achieve this frame rate, DaVinci2K could sample fluorescence at 14-bit depth with a frame size of 128X14 pixels comprising 4 of the 16 sub-sensors (Figure 1C, left), whereas Kinetix sampled fluorescence at 8-bit depth with a frame size of 208X70 pixels (Figure 1D, left). We tested the ability to discriminate fluorescence transients associated with APs elicited in the soma (Figure 1C-D, top right). Single-trial raw digital signals from two bright pixels in the AIS are shown in the red middle-right traces for DaVinci2K (Figure 1C) and Kinetix (Figure 1D). The 14-bit depth of DaVinci2K enables using high laser power intensity to excite fluorescence without reaching the saturating well capacity of the pixel. In contrast, weaker power intensity had to be used for Kinetix since the effective pixel well capacity is ~ 200 photoelectrons. The result was that SNR, due to intrinsic photon noise, is higher for DaVinci2K. This advantage is mitigated by the larger photobleaching resulting from the use of more powerful intensity, a phenomenon that can pose additional limitations in terms of photodamage of the tissue. We then averaged fluorescence in the two single-trials, from progressively larger regions-of-interest (ROIs) illustrated in Figures 1C-D (right): Red square, single pixel; blue square, 2X2 pixels; green rectangle, 2X8 pixels; and purple rectangle, 2X16 pixels. Then, from these averages, we calculated the $\Delta F/F_0$ signal (Figure 1C-D, bottom-right). To visually compare the two recordings, averages from DaVinci2K were corrected for photobleaching, a procedure that was not necessary for averages from Kinetix. Consistently with the fact that both devices achieve measurements where the SNR is limited by the photon noise, $\Delta F/F_0$ signals from DaVinci2K are less noisy than those from Kinetix. In addition, measurements at 14-bit depth enable simultaneous recordings from pixels with high variability in brightness, whereas measurements at 8-bit depth can be practically achieved only from pixels with comparable brightness. In contrast, 8-bit acquisitions with Kinetix enable recordings with a much larger frame size. In summary, we show the ability of both cameras to resolve $\Delta F/F_0$ signals of 1−10% at very high spatiotemporal resolution, with advantages and limitations that should guide the choice of the device on the basis of the application.

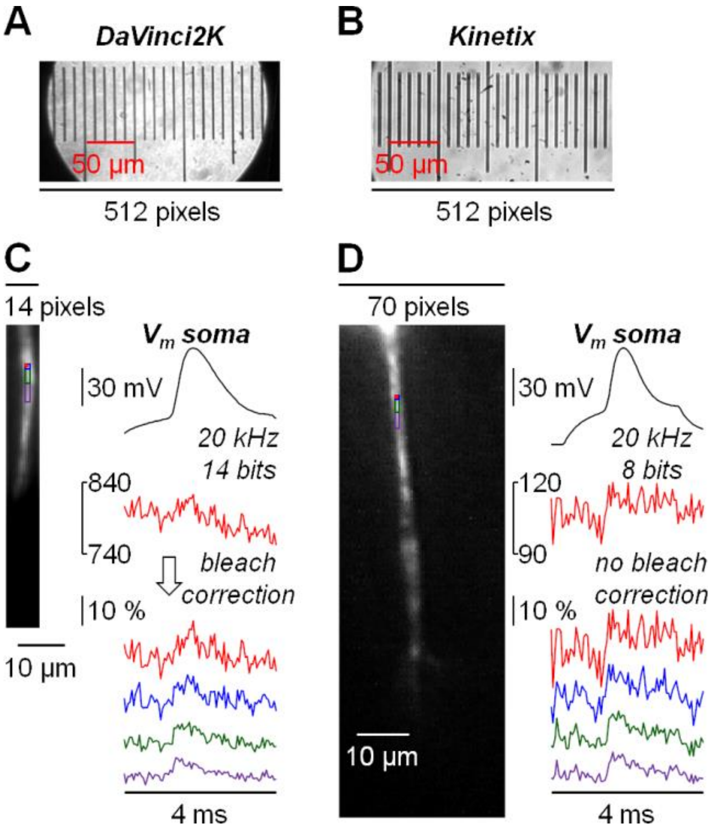

Figure 1. Examples of V_m imaging with DaVinci2K and Kinetix CMOS cameras. **A-B)** Images of a micrometer (512 pixels x-direction) captured with a 60X objective after 0.5X demagnification with DaVinci2K CMOS or 0.25X demagnification with Kinetix CMOS. The effective pixel length is ~ 0.5 µm for DaVinci2K and ~ 0.43 µm for Kinetix. **C)** On the left is a 90°-rotated fluorescence frame with DaVinci2K (from the VSD JPW1114) at the size that could be acquired at 20 kHz and 14-bit depth (128X14 pixels). On the right is an evoked somatic AP (top trace) and fluorescence transients (at 20 kHz) from various coloured ROIs. The middle (red) trace is raw fluorescence from a single pixel and scale indicates the digital number (from 14-bit digitisation). The bottom traces are obtained after correcting for bleaching and correspond to $\Delta F/F_0$ signals by averaging fluorescence in the coloured regions. **D)** Same as (C) with Kinetix at the size that could be acquired at 20 kHz and 8-bit depth (208 X 70 pixels). In this case, the middle (red) trace is raw fluorescence from a single pixel, and scale indicates the digital number from 8-bit digitisation. Bottom traces are obtained without correcting for bleaching. Both examples are from single trials.

4. Conclusions and perspectives

In the last decade or so, CMOS technology became the state-of-the-art for high-speed neuronal functional imaging. Its superiority with respect to previous technologies is due to its intrinsic way of functioning. I analysed ways to further boost the acquisition rate of CMOS imaging from two cameras that are in use in my laboratory. One way, exploited by DaVinci2K and previously used in CCD technology, is to build sensors composed by multiple sub-sensors in order to parallelise the acquisition process. By designing geometries that permit the selection of rectangles, including all sub-sensors, the camera can increase the acquisition rate by the number of sub-sensors. A caveat of this approach is the financial cost needed for enabling parallel processing. A second way, exploited by Kinetix, is to decrease the bit depth of the acquired images. The limitation of this approach is the decrease in dynamic range that can be critical in some experimental conditions. Notably, Kinetix acquires 8-bit images in quasi "photon counting" mode, where each pixel saturates at ~ 200 photoelectrons. The dynamic range is afterwards increased by performing offline binning, but since each pixel must acquire a signal of nearly the same intensity, this limits the applicability to experiments where emitted light from all sites of interest is uniform. New CMOS cameras with comparable speed at 10-bit depth and variable gain exist, mitigating the limitation of uniform emitted light. Thus, although these cameras have not been used for fast functional imaging, the cameras analysed in this review may not be any more the state-of-the-art. On the other hand, another limitation is given by the necessary SNR, which is given by the number of photons that can be practically collected by each pixel at a given exposure time (Equation 2), and this is associated with the area covered by a pixel. It was seen that a pixel size > 10 µm is somehow desirable to acquire with a resolution in the order of 1µm/pixel. A very promising approach that goes in this direction is the introduction of programmable-exposure (PE) CMOS devices that optimise the SNR, particularly in frequent scenarios of high dynamic range [42]. This is important because it is typically the case when CMOS cameras are used to record signals from genetically encoded voltage indicators [43,44]. A final consideration for the perspective improved CMOS sensors in the near future is on the cost of developing these devices, which is in the M€ region. At present, the market of biological and biomedical research is insufficient to justify developments uniquely dedicated to these applications. While investments for developing new sensors are targeted to a variety of applications, from military to industrial control, scientific cameras are produced from available devices. Beyond biology, very recent CMOS camera exploitations in scientific research include astrophysics [45], material science [46], and RAMAN spectroscopy [47], but at this stage, these applications only appear insufficient for investing in novel devices. This aspect should be considered among present limitations.

Use of generative-AI tools declaration

The author declare they have not used Artificial Intelligence (AI) tools in the creation of this article.

Acknowledgments

Data used in Figure 1 were produced by Fatima Abbas and supported by the *Agence Nationale de la Recherche* through two grants (ANR-21-CE18-0042 – Nav12RESCUE and Labex *Ion Channels Science and Therapeutics:* program number ANR-11-LABX-0015).

Conflict of interest

The author declares no conflict of interest.

References

1. Sepehri Rad M, Choi Y, Cohen LB, et al. (2017) Voltage and calcium imaging of brain activity. *Biophys J* 113: 2160–2167. https://doi.org/10.1016/j.bpj.2017.09.040
2. Fritzky L, Lagunoff D (2013) Advanced methods in fluorescence microscopy. *Anal Cell Pathol* 36: 5–17. https://doi.org/10.3233/ACP-120071
3. Conchello JA, Lichtman JW (2005) Optical sectioning microscopy. *Nat Methods* 2: 920–931. https://doi.org/10.1038/nmeth815
4. Rubart M (2004) Two-photon microscopy of cells and tissue. *Circ Res* 95: 1154–1166. https://doi.org/10.1161/01.RES.0000150593.30324.42
5. Homma R, Baker BJ, Jin L, et al. (2009) Wide-field and two-photon imaging of brain activity with voltage- and calcium-sensitive dyes. *Philos Trans R Soc Lond B Biol Sci* 364: 2453–2467. https://doi.org/10.1098/rstb.2009.0084
6. Orbach HS, Cohen LB, Grinvald A (1985) Optical mapping of electrical activity in rat somatosensory and visual cortex. *J Neurosci* 5: 1886–1895. https://doi.org/10.1523/JNEUROSCI.05-07-01886.1985
7. Ross WN, Werman R (1987) Mapping calcium transients in the dendrites of Purkinje cells from the guinea-pig cerebellum in vitro. *J Physiol* 389: 319–336. https://doi.org/10.1113/jphysiol.1987.sp016659
8. Wu JY, London JA, Zecevic D, et al. (1988) Optical monitoring of activity of many neurons in invertebrate ganglia during behaviors. *Experientia* 44: 369–376. https://doi.org/10.1007/BF01940529
9. Zecević D (1996) Multiple spike-initiation zones in single neurons revealed by voltage-sensitive dyes. *Nature* 381: 322–325. https://doi.org/10.1038/381322a0
10. Takamatsu T, Wier WG (1990) High temporal resolution video imaging of intracellular calcium. *Cell Calcium* 11: 111–120. https://doi.org/10.1016/0143-4160(90)90064-2
11. Lasser-Ross N, Miyakawa H, Lev-Ram V, et al. (1991) High time resolution fluorescence imaging with a CCD camera. *J Neurosci Methods* 36: 253–261. https://doi.org/10.1016/0165-0270(91)90051-Z
12. Mammano F, Canepari M, Capello G, et al. (1999) An optical recording system based on a fast CCD sensor for biological imaging. *Cell Calcium* 25: 115–123. https://doi.org/10.1054/ceca.1998.0013
13. Canepari M, Mammano F, Kachalsky SG, et al. (2000) GABA- and glutamate-mediated network activity in the hippocampus of neonatal and juvenile rats revealed by fast calcium imaging. *Cell Calcium* 27: 25–33. https://doi.org/10.1054/ceca.1999.0086
14. Ross WN, Miyazaki K, Popovic MA, et al. (2015) Imaging with organic indicators and high-speed charge-coupled device cameras in neurons: some applications where these classic techniques have advantages. *Neurophotonics* 2: 021005. https://doi.org/10.1117/1.NPh.2.2.021005
15. Callaway JC, Lasser-Ross N, Ross WN (1995) IPSPs strongly inhibit climbing fiber-activated [Ca2+]i increases in the dendrites of cerebellar Purkinje neurons. *J Neurosci* 15: 2777–2787. https://doi.org/10.1523/JNEUROSCI.15-04-02777.1995

16. Takashima I, Ichikawa M, Iijima T (1999) High-speed CCD imaging system for monitoring neural activity in vivo and in vitro, using a voltage-sensitive dye. *J Neurosci Methods* 91: 147−159. https://doi.org/10.1016/S0165-0270(99)00093-X
17. Larkum ME, Watanabe S, Nakamura T, et al. (2003) Synaptically activated Ca^{2+} waves in layer 2/3 and layer 5 rat neocortical pyramidal neurons. *J Physiol* 549: 471−488. https://doi.org/10.1113/jphysiol.2002.037614
18. Antic SD (2003) Action potentials in basal and oblique dendrites of rat neocortical pyramidal neurons. *J Physiol* 550: 35−50. https://doi.org/10.1113/jphysiol.2002.033746
19. Djurisic M, Antic S, Chen WR, et al. (2004) Voltage imaging from dendrites of mitral cells: EPSP attenuation and spike trigger zones. *J Neurosci* 24: 6703−6714. https://doi.org/10.1523/JNEUROSCI.0307-04.2004
20. Milojkovic BA, Zhou WL, Antic SD (2007) Voltage and calcium transients in basal dendrites of the rat prefrontal cortex. *J Physiol* 585: 447−468. https://doi.org/10.1113/jphysiol.2007.142315
21. Djurisic M, Popovic M, Carnevale N, et al. (2008) Functional structure of the mitral cell dendritic tuft in the rat olfactory bulb. *J Neurosci* 28: 4057−4068. https://doi.org/10.1523/JNEUROSCI.5296-07.2008
22. Foust AJ, Yu Y, Popovic M, et al. (2011) Somatic membrane potential and Kv1 channels control spike repolarization in cortical axon collaterals and presynaptic boutons. *J Neurosci* 31: 15490−15498. https://doi.org/10.1523/JNEUROSCI.2752-11.2011
23. Popovic MA, Foust AJ, McCormick DA, et al. (2011) The spatio-temporal characteristics of action potential initiation in layer 5 pyramidal neurons: a voltage imaging study. *J Physiol* 589: 4167−4187. https://doi.org/10.1113/jphysiol.2011.209015
24. Jaafari N, Canepari M (2016) Functional coupling of diverse voltage-gated Ca^{2+} channels underlies high fidelity of fast dendritic Ca^{2+} signals during burst firing. *J Physiol* 594: 967−983. https://doi.org/10.1113/JP271830
25. Short SM, Oikonomou KD, Zhou WL, et al. (2017) The stochastic nature of action potential backpropagation in apical tuft dendrites. *J Neurophysiol* 118: 1394−1414. https://doi.org/10.1152/jn.00800.2016
26. Ait Ouares K, Canepari M (2020) The origin of physiological local mGluR1 supralinear Ca^{2+} signals in cerebellar Purkinje neurons. *J Neurosci* 40: 1795−1809. https://doi.org/10.1523/JNEUROSCI.2406-19.2020
27. Ahrens MB, Orger MB, Robson DN, et al. (2013) Whole-brain functional imaging at cellular resolution using light-sheet microscopy. *Nat Methods* 10: 413−420. https://doi.org/10.1038/nmeth.2434
28. Filipis L, Ait Ouares K, Moreau P, et al. (2018) A novel multisite confocal system for rapid Ca^{2+} imaging from submicron structures in brain slices. *J Biophotonics* 11: e201700197. https://doi.org/10.1002/jbio.201700197
29. Kim Y, Lee U, Choi C, et al. (2020) Release mode dynamically regulates the RRP refilling mechanism at individual hippocampal synapses. *J Neurosci* 40: 8426−8437. https://doi.org/10.1523/JNEUROSCI.3029-19.2020
30. Xiao S, Lowet E, Gritton HJ, et al. (2021) Large-scale voltage imaging in behaving mice using targeted illumination. *iScience* 24: 103263. https://doi.org/10.1016/j.isci.2021.103263
31. Filipis L, Canepari M (2021) Optical measurement of physiological sodium currents in the axon initial segment. *J Physiol* 599: 49−66. https://doi.org/10.1113/JP280554

32. Mendonça PRF, Tagliatti E, Langley H, et al. (2022) Asynchronous glutamate release is enhanced in low release efficacy synapses and dispersed across the active zone. *Nat Commun* 13: 3497. https://doi.org/10.1038/s41467-022-31070-4
33. Filipis L, Blömer LA, Montnach J, et al. (2023) Nav1.2 and BK channel interaction shapes the action potential in the axon initial segment. *J Physiol* 601: 1957−1979. https://doi.org/10.1113/JP283801
34. Ahanonu B, Crowther A, Kania A, et al. (2024) Long-term optical imaging of the spinal cord in awake behaving mice. *Nat Methods* 21: 2363−2375. https://doi.org/10.1038/s41592-024-02476-3
35. Huang YC, Chen HC, Lin YT, et al. (2024) Dynamic assemblies of parvalbumin interneurons in brain oscillations. *Neuron* 112: 2600−2613. https://doi.org/10.1016/j.neuron.2024.05.015
36. Abbas F, İpek ÖY, Moreau P, et al. (2025) Neuronal imaging at 8-bit depth to combine high spatial and high temporal resolution with acquisition rates up to 40 kHz. *J Biophotonics* 18: e202400513. https://doi.org/10.1002/jbio.202400513
37. Marosi EL, Arszovszki A, Brunner J, et al. (2023) Similar presynaptic action potential-calcium influx coupling in two types of large mossy fiber terminals innervating CA3 pyramidal cells and hilar mossy cells. *eNeuro* 10: ENEURO.0017-23.2023. https://doi.org/10.1523/ENEURO.0017-23.2023
38. Brunner J, Arszovszki A, Tarcsay G, et al. (2024) Axons compensate for biophysical constraints of variable size to uniformize their action potentials. *Plos Biol* 22: e3002929. https://doi.org/10.1371/journal.pbio.3002929
39. Ortkrass H, Müller M, Engdahl AK, et al. (2024) High sensitivity cameras can lower spatial resolution in high-resolution optical microscopy. *Nat Commun* 15: 8886. https://doi.org/10.1038/s41467-024-53198-1
40. Nguyen JP, Shipley FB, Linder AN, et al. (2016) Whole-brain calcium imaging with cellular resolution in freely behaving *Caenorhabditis elegans*. *Proc Natl Acad Sci USA* 113: E1074−81. https://doi.org/10.1073/pnas.1507110112
41. Obara K, Ebina T, Terada SI, et al. (2023) Change detection in the primate auditory cortex through feedback of prediction error signals. *Nat Commun* 14: 6981. https://doi.org/10.1038/s41467-023-42553-3
42. Zhang J, Newman J, Wang Z, et al. (2024) Pixel-wise programmability enables dynamic high-SNR cameras for high-speed microscopy. *Nat Commun* 15: 4480. https://doi.org/10.1038/s41467-024-48765-5
43. Adam Y, Kim JJ, Lou S, et al. (2019) Voltage imaging and optogenetics reveal behaviour-dependent changes in hippocampal dynamics. *Nature* 569: 413−417. https://doi.org/10.1038/s41586-019-1166-7
44. Xiao S, Cunningham WJ, Kondabolu K, et al. (2024) Large-scale deep tissue voltage imaging with targeted-illumination confocal microscopy. *Nat Methods* 21: 1094−1102. https://doi.org/10.1038/s41592-024-02275-w
45. Dowd K, Doyle E, Dunne P (2025) Near infra-red absorption spectroscopy for astrophysically significant ions. *Exp Astron* 60: 7. https://doi.org/10.1007/s10686-025-10009-9
46. Ma Q, Liu Z, Zhang T, et al. (2024) Multielement simultaneous quantitative analysis of trace elements in stainless steel via full spectrum laser-induced breakdown spectroscopy. *Talanta* 272: 125745. https://doi.org/10.1016/j.talanta.2024.125745

47. Klement WJN, Leproux P, Browne WR, et al. (2025) CMOS and CCD detection in Raman spectroscopy: A comparison using spontaneous and multiplex coherent anti-stokes Raman scattering (CARS). *J Raman Spectrosc* 56: 933−938. https://doi.org/10.1002/jrs.6773